Modern radio engineering and telecommunication systems

Современные радиотехнические и телекоммуникационные системы

UDC 621.314.6; 621.373.5
https://doi.org/10.32362/2500-316X-2025-13-1-103-114
EDN UORVPM

RESEARCH ARTICLE

Resonant power supply for high-power microwave devices

Damir R. Hafizov [1, 2, @], Ilya N. Lobov [1], Leonid Y. Fetisov [2]

[1] *NPO "Almaz", Moscow, 125190 Russia*
[2] *MIREA – Russian Technological University, Moscow, 119454 Russia*
[@] *Corresponding author, e-mail: hafizov98@yandex.ru*

Abstract

Objectives. The ever-increasing demands on the technical parameters of microwave radio transmission devices necessitate a search for ways of improving their efficiency and reliability, as well as means for reducing their weight and size parameters. Since such requirements largely relate to secondary power supplies, the present work set out to develop secondary power supplies for the cathode heating and bias circuits of a floating-drift multibeam klystron capable of operating at a high potential of the klystron cathode and providing stable voltage in all operating modes.

Methods. In order to calculate the parameters of the resonant circuit, the first harmonic approximation method is used.

Results. Approaches for designing secondary supplies are described along with the method for developing the cathode heating and bias supplies for a floating-drift multipath klystron. The calculation method used for testing the design of the transformer windings is presented. The design avoids the use of chokes as separate elements by integrating them inside a magnetic system and providing isolation by high potential of the secondary winding. The results of testing the power supply using complex test bench waveforms are given along with the main obtained parameters. The operation of the power supply is demonstrated in switching mode at zero voltage for the minimum, nominal, and maximum input voltages in the range of the inductive resistance of the circuit when the voltage phase precedes the current phase.

Conclusions. The calculated efficiencies of the presented cathode heating and bias supplies are 85% and 92%, respectively. The developed supplies, which have smaller dimensions than their transformer analogues, allow a stable output voltage to be maintained when the input voltage varies, while the use of the soft start method allows the life of the klystron to be extended.

Keywords: voltage converter, resonant converter, power supply of microwave devices, pulse transformer, klystron

• **Submitted:** 11.02.2024 • **Revised:** 14.06.2024 • **Accepted:** 11.12.2024

For citation: Hafizov D.R., Lobov I.N., Fetisov L.Y. Resonant power supply for high-power microwave devices. *Russian Technological Journal.* 2025;13(1):103–114. https://doi.org/10.32362/2500-316X-2025-13-1-103-114, https://elibrary.ru/UORVPM

Financial disclosure: The authors have no financial or proprietary interest in any material or method mentioned.

The authors declare no conflicts of interest.

НАУЧНАЯ СТАТЬЯ

Резонансный источник электропитания для мощных сверхвысокочастотных устройств

Д.Р. Хафизов [1, 2, @],
И.Н. Лобов [1],
Л.Ю. Фетисов [2]

[1] *НПО «Алмаз», Москва, 125190 Россия*
[2] *МИРЭА – Российский технологический университет, Москва, 119454 Россия*
[@] *Автор для переписки, e-mail: hafizov98@yandex.ru*

Резюме

Цели. Постоянно растущие требования к техническим параметрам радиопередающих сверхвысокочастотных (СВЧ) устройств вызывают необходимость искать способы повышения их эффективности и надежности, а также уменьшения массогабаритных показателей. Эти требования в значительной мере касаются источников вторичного электропитания. Целью данной работы является разработка источников вторичного электропитания цепей накала и смещения для пролетного многолучевого клистрона, способных работать под высоким потенциалом катода клистрона и обеспечивать стабильное напряжение во всех рабочих режимах.

Методы. Для расчета параметров резонансного контура использован метод аппроксимации первой гармоники.

Результаты. Описан метод разработки источников вторичного электропитания, разработаны источники питания накала и смещения для пролетного многолучевого клистрона. Представлен метод расчета и апробирована конструкция обмоток трансформатора, позволяющие отказаться от использования дросселей как отдельных элементов путем их интеграции внутри одной магнитной системы и обеспечить развязку по высокому потенциалу вторичной обмотки. Проведены испытания источника питания в составе комплексного испытательного моделирующего стенда, получены осциллограммы основных параметров. Показана работа источника питания в режиме переключения при нулевом напряжении для минимального, номинального и максимального входного напряжения в области с индуктивным сопротивлением контура, когда фаза напряжения опережает фазу тока.

Выводы. Коэффициенты полезного действия источников накала и смещения составили 85% и 92% соответственно. Разработанные источники имеют меньшие габариты по сравнению с трансформаторными аналогами и позволяют поддерживать стабильное выходное напряжение при изменении входного напряжения, а использование метода плавного пуска позволит продлить срок службы клистрона.

Ключевые слова: преобразователь напряжения, резонансный преобразователь, электропитание СВЧ-устройств, импульсный трансформатор, клистрон

• **Поступила:** 11.02.2024 • **Доработана:** 14.06.2024 • **Принята к опубликованию:** 11.12.2024

Для цитирования: Хафизов Д.Р., Лобов И.Н., Фетисов Л.Ю. Резонансный источник электропитания для мощных сверхвысокочастотных устройств. *Russian Technological Journal.* 2025;13(1):103–114. https://doi.org/10.32362/2500-316X-2025-13-1-103-114, https://elibrary.ru/UORVPM

Прозрачность финансовой деятельности: Авторы не имеют финансовой заинтересованности в представленных материалах или методах.

Авторы заявляют об отсутствии конфликта интересов.

INTRODUCTION

Klystrons and travelling wave tubes are powerful amplifying microwave radio transmission devices that convert electron flux into microwave oscillation energy [1]. These devices are used as output power amplifiers in radio transmitting equipment [2–4]. The ever-increasing requirements for the specifications of microwave radio transmission devices necessitate the search for ways to improve their efficiency and reliability, as well as to reduce their weight and size parameters. These requirements are largely related to the secondary power supplies.

Today, power supplies for microwave equipment use network transformers operating at frequencies of 50 and 400 Hz. The major disadvantage of such power supplies is their large overall size, as determined by the size and weight of the power transformer, filter, and voltage stabilizer components. Voltage stabilizers are used to maintain high stability of the output voltage in the secondary circuit with some reduction in the efficiency of the source.

The most commonly used devices are pulsed power supplies in which voltage stabilization is provided by the control circuit to regulate the power transfer to the transformer on the primary side. The use of high frequency pulse transformers, which can operate at frequencies above 10^5 Hz, allows the overall size of the device to be reduced; as compared to a mains transformer having the same total transformer core power, the weight and size of a pulse transformer is significantly less.

Pulse-width modulation (PWM) converters are used as the basis for switching power supplies that convert the rectified mains voltage into a square-wave pulse voltage allowing the output voltage to be regulated by changing the duration of the pulses. PWM converters are characterized by abrupt changes in current and voltage, which cause high switching losses and limit the upper operating frequency of the converter. On the other hand, large rates of change in current and voltage cause electromagnetic interference in a wide range of the spectrum, thus precluding the use of pulse power supplies for high power microwave devices [5].

The aim of the present work is to develop secondary power supplies for the cathode heating and bias circuits of a floating-drift multibeam klystron capable of operating at high klystron cathode potentials of about 25 kV.

RESONANT POWER SUPPLIES

A resonant converter power supply, whose output voltage is almost sinusoidal due to the use of an LC circuit in the converter, avoids the disadvantages described above by reducing the noise level in comparison with PWM converters [5, 6]. At the same time, the use of resonant circuits makes it possible to implement the zero-voltage method for switching transistors when the in-phase circuit current lags behind the voltage to significantly reduce switching losses [7]. While resonant converters have various topologies, they are all based on a similar operating principle [8].

A series-parallel LLC converter is described in [9]. The series-parallel resonant converter is a preferred topology in the design of high voltage power supplies due to its ability to smoothly switch over a wide range of operating frequencies [10]. The circuit diagram of a half-bridge resonant LLC converter is shown in Fig. 1.

The circuit contains the input voltage source V_{in}, transistors VT1 and VT2 connected by a half-bridge circuit, resonant capacitor C_r, series inductor L_r, transformer T with ratio n and shunt parallel inductor L_{sh}. In practice, the parallel inductance can be eliminated from the circuit as a separate physical element. This can be achieved by using the intrinsic magnetizing inductance L_m of the transformer, whose value is achieved by introducing an air gap in the transformer core as discussed later. The secondary voltage is rectified by diodes VD1 and VD2 and then fed to a capacitive smoothing filter formed by capacitor C1 and resistor R1 as an equivalent output load. For high secondary current values, synchronous rectifiers with field MOSFETs[1] are used as voltage rectifiers. Due to the low resistance of the drain-to-source channel, these rectifiers are more efficient than diodes [11]. The soft-start method is used to limit the inrush current at switch-on [12, 13].

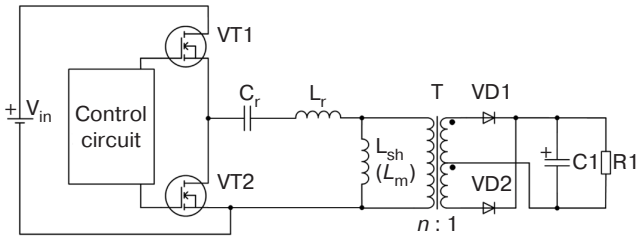

Fig. 1. Circuit diagram of a resonant half-bridge LLC converter. Here and in the following figures, the designations of the circuit elements correspond to those adopted in GOST 2.710-81[2]

In the resonant circuit, the current lags behind the voltage. This allows transistors to switch at zero voltage while current flows through the antiparallel diode of the transistor [14]. The sinusoidal voltage is applied to the load via the transformer. The output voltage is adjusted by changing the operating frequency of the transistors,

[1] Metal–oxide–semiconductor.

[2] GOST 2.710-81. Interstate Standard. *Unified system for design documentation. Alpha-numerical designations in electrical diagrams*. Moscow: Izd. Standartov; 1985 (in Russ.).

thus changing the operating mode of the converter. Due to the presence of both series and parallel components, the converter has a lower and an upper resonant frequency [15]. The lower frequency is determined by the elements L_r and C_r together with the value L_m, while the upper frequency is due to the elements L_r and C_r.

RESONANT CIRCUIT CALCULATION

The cathode heating power supply parameters are calculated using the first harmonic approximation method [16]. The power supply is fed from the 220 V ± 10% mains at a frequency of 400 Hz. The output voltage of the source is (13 ± 0.5) V, while the nominal current is 12 A, and the maximum current does not exceed 15 A. The transformation ratio n at the nominal input voltage is determined when the transfer coefficient M of the circuit is equal to one.

$$n = M\frac{V_{in}/2}{V_{out}} = 12, \quad (1)$$

where nominal input voltage V_{in} = 311 V and output voltage V_{out} = 13 V.

The equivalent alternating current resistance R_{ac} is defined in the following way:

$$R_{ac} = \frac{8n^2V_{out}}{\pi^2 I_{out}} = 126 \text{ Ohm}. \quad (2)$$

The following expressions are used to determine the maximum and minimum values of the transmission coefficients:

$$M_{min} = \frac{nV_{out\_min}}{V_{in\_max}/2} = 0.87, \quad (3)$$

$$M_{max} = \frac{nV_{out\_max}}{V_{in\_min}/2} = 1.15, \quad (4)$$

where V_{out_min} = 12.5 V, V_{out_max} = 13.5 V, V_{in_min} = 279 V, V_{in_max} = 341 V.

The resonant frequency of the circuit is determined by the following equation:

$$f_r = \frac{1}{2\pi\sqrt{L_rC_r}}. \quad (5)$$

The operating frequency of the power supply which is chosen on the basis of the specifications for the design of the source for the radar station, must not exceed 100 kHz.

The resonance frequency value is chosen such that the resonance capacitor capacitance is equal to or a multiple of the standard value, e.g., E24 series. The resonance frequency chosen is f_r = 80 kHz.

The following equation determines the capacitance value of capacitor C_r:

$$C_r = \frac{1}{2\pi QfR_{ac}} = 22 \text{ nF}, \quad (6)$$

where the quality factor (Q factor) of the circuit is Q = 0.7, while the switching frequency is f = 80 kHz.

The Q value is selected on the basis of the maximum and minimum transmission coefficient. This is done by plotting several transmission characteristics with different Q values on the same graph. On this graph, horizontal lines are drawn corresponding to the maximum M_{max} and minimum M_{min} transmission coefficients. The transmission coefficient curve is selected from those plotted that intersects both horizontal lines in the selected frequency range is selected.

High Q values reduce the peak transmission coefficient. However, a reserve of approximately 15% of the peak transmission coefficient is required to ensure zero voltage switching over the entire operating frequency range. The optimum value is therefore Q = 0.7.

The inductance L_r is calculated using the following equation:

$$L_r = \frac{1}{(2\pi f)^2 C_r} = 181 \text{ μH}. \quad (7)$$

To simplify inductance calculations, L_m and L_r are combined into a total inductance parameter. Total inductance is defined as follows:

$$L_n = \frac{L_m}{L_r}. \quad (8)$$

The L_n value is selected by plotting the circuit transfer coefficient curves for different L_n values. As L_n decreases, the peak transfer coefficient increases along with a decrease in the magnetizing inductance and increase in the magnetizing current; therefore, the optimum value of L_n = 3...7. In the calculations, the value L_n = 3 and the value of the magnetizing inductance L_m = 543 μH are used.

The following expression can be used to analyze changes in the transfer characteristic when the resonant circuit parameters are changed:

$$M = \left| \frac{L_n f_n^2}{[(L_n + 1) f_n^2 - 1] + j[(f_n^2 - 1) f_n Q L_n]} \right|, \quad (9)$$

where f_n is the ratio of switching frequency f to the circuit resonant frequency f_r,

$$f_n = \frac{f}{f_r}. \quad (10)$$

With known values L_r, C_r, and R_{ac}, the circuit Q factor is defined as follows:

$$Q = \frac{\sqrt{L_r / C_r}}{R_{ac}}. \quad (11)$$

The transfer characteristics of the converter are plotted for different circuit Q factors using the above equations (Fig. 2).

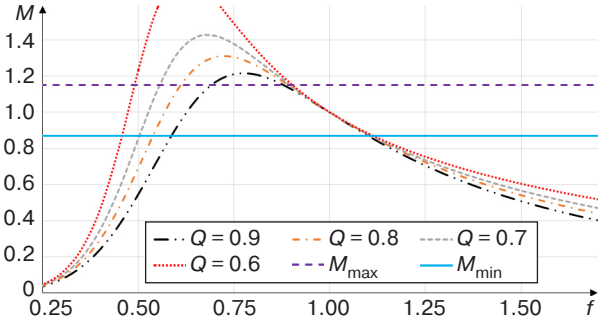

Fig. 2. Circuit transmission coefficient as a function of the circuit Q factor (current frequency normalized to the resonant frequency)

Depending on the region of the transfer characteristic in which the converter operates, different switching modes can be implemented: at zero current and at zero voltage [17]. If the operating frequency of the converter is to the left of the peak factor M, the converter operates in the region where the capacitance of the converter is primary. However, when operating with a capacitive load, the current in the circuit is ahead of the voltage and the zero-current switching mode is implemented. Operating in this region results in high losses due to the transistors switching under harsh conditions. If the operating frequency of the converter is to the right of the peak factor M, the inductive impedance is dominant. However, when operating in the inductive region, the voltage in the circuit is higher than the current. Therefore, it is in this operating region that the zero-voltage switching mode is implemented, allowing the transistors to switch with minimum loss. Consequently, the optimum operating region of the converter is to the right of the peak factor M.

INTEGRATED MAGNETIC SYSTEM

The resonant circuit consists of three electromagnetic components comprising a transformer T, parallel inductor L_{sh} (L_m), and series inductor L_r. Although each of these components is manufactured on a separate core (magnetic core), it would be more rational to integrate them in a magnetic system based on a transformer. The possibility of integrating the components within a magnetic system is justified by the equivalent circuit of a two-winding transformer in which the output load is reduced to the primary winding [18]. The inductance L_r can be replaced by the scattering inductance L_{S1} of the primary winding while the parallel inductance L_{sh} can be replaced by the transformer magnetizing inductance L_m [19].

For correct operation of the circuit while preserving the possibility of implementing switching at zero voltage, the magnetizing inductance should be within $(3...8)L_r$. This can be achieved by introducing a nonmagnetic gap in the transformer. The core used in the calculation is the Epcos core N87 (size ER 42/22/15, magnetic permeability $\mu = 2200$, and saturation induction $B_s = 0.49$ T).

The magnetizing inductance for gap transformers is defined as follows [20]:

$$L_m = \frac{\mu_{eff} \mu_0 N_1^2 S_c}{l_{av}}, \quad (12)$$

where μ_{eff} is the effective magnetic permeability; μ_0 is the magnetic constant; N_1 is the number of turns of the primary winding; S_c is the cross-sectional area of the magnetic core; l_{av} is the length of the central line of the magnetic core.

The effective magnetic permeability is the magnetic permeability of the core material with a gap, which is defined as follows:

$$\mu_{eff} = \frac{1}{\frac{1}{\mu} + \frac{l_g}{l_{av}}}, \quad (13)$$

where μ is the magnetic permeability of the material; l_g is the length of the nonmagnetic gap.

The number of turns of the primary winding is determined by the following equation:

$$N_1 = \frac{n(V_{out} + V_f)}{2 f_{min} M_{min} B S_c} = 20, \quad (14)$$

where the direct voltage drop across the rectifier diode $V_f = 0.6$ V, the minimum operating frequency $f_{min} = 72$ kHz, and the value of maximum induction $B = 0.4$ T.

The minimum operating frequency f_{min} is determined from the graph (Fig. 2).

The value of the maximum induction is determined from the value of the core saturation induction using the following equation:

$$B = 0.8B_s = 0.4 \text{ T}. \quad (15)$$

Taking into account the transformation ratio, the number of secondary winding turns $N_2 = 2$.

Substituting (13) into (12), the value of the nonmagnetic gap is calculated to obtain the required magnetizing inductance, as follows:

$$l_g = \frac{\mu\mu_0 N_1^2 S_c - l_{av} L_m}{\mu L_m} = 0.11 \text{ mm}, \quad (16)$$

where the cross-sectional area of the magnetic core S_c = 170 mm^2, and the length of the center line of the magnetic core l_{av} = 99 mm.

The scattering inductance of the primary winding is that part of the inductance which is not connected by the common magnetic flux to the secondary winding and the magnetic core, while the magnetic flux is short-circuited through the air. For *W*- and *U*-shaped magnetic circuits, the scattering inductance can be calculated using the following equation for an inductor without a magnetic core:

$$L_{S1} = \frac{\mu_0 N_1^2 S_{i.s.}}{h_w}, \quad (17)$$

where the area of inductive system $S_{i.s.}$ is the effective area covered by the current, excluding the magnetic core area; h_w is the winding height.

The effective area is determined by the following equation:

$$S_{i.s.} = l_{w1\_av}\delta_{w1}, \quad (18)$$

where l_{w1_av} is the average primary winding turn length; δ_{w1} is the distance from the average primary winding turn to the magnetic core.

Equations (17) and (18) show that in order to increase the scattering inductance, it is necessary to separate the primary and secondary windings on the transformer frame by increasing the number of turns of the winding and its thickness, as well as reducing the length of the winding on the magnetic core.

The scattering inductance close to the calculated value can be obtained by using the sectional winding method shown in Fig. 3. Unlike the winding method, where the primary and secondary windings are layered along the entire length of the frame, the sectional method gives the highest value of scattering inductance.

Once the transformer has been wound, it is necessary to check that the inductance of the primary winding is equal to the value of the total inductance $L_m + L_r$. If it differs from the calculated value, the difference can be compensated by adjusting the core gap. The next step is to check that the value obtained for the scattering inductance is within 10% of the calculated value. This is done by short-circuiting all the output windings and measuring the inductance of the primary winding. If the measured value differs from the calculated value by more than 10%, the transformer should be remanufactured. If all parameters match the calculated values, the transformer is suitable for use.

While the primary and secondary sectional winding method is suitable for achieving relatively low output voltage levels, it is not suitable for achieving the high voltages required by bias sources where output voltages can range from units to tens of kilovolts and ensuring electrical robustness is of paramount importance.

For high voltage levels, a *U*-shaped core is used with the primary and secondary windings separated by a certain distance. The primary and secondary windings are fixed on opposite core bars, while the secondary winding is divided into separate sections. After winding, the transformer windings are filled with insulating compound (Fig. 4).

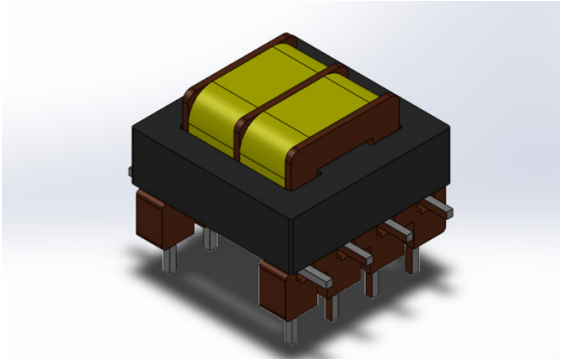

Fig. 3. Winding arrangement of the cathode heating transformer

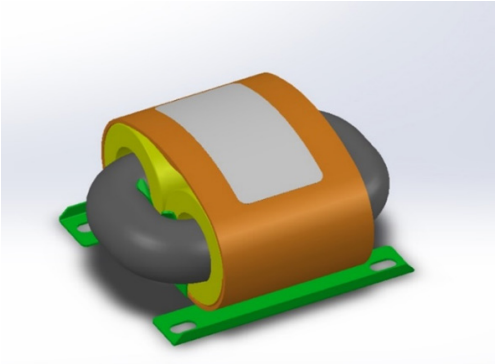

Fig. 4. Example of high voltage transformer layout for powering the klystron bias circuit

TESTING THE DEVELOPED SOURCE

The cathode heating and bias power supplies for the floating-drift multibeam klystron are designed according to the described method.

The source of the cathode heating circuit has the following parameters: cathode heating voltage $U_{cath.heat.} = 13$ V; nominal cathode heating current $I_{cath.heat.} = 12$ A; resonance capacitor capacity $C_r = 22$ nF; resonance inductance $L_r = 182$ μH; and resonance frequency $f_r = 80$ kHz. The soft start method is implemented in the source to extend the life of the klystron.

The klystron bias source provides voltage $U_{bias} = 6$ kV at a current not exceeding than $I_{bias} = 100$ mA, resonant frequency $f_r = 80$ kHz, resonant capacitor capacitance $C_r = 68$ nF, and resonant inductance $L_r = 58$ μH.

The development of such a source is complicated by the electrical robustness of the transformer at the high potential of the secondary winding, which is below the cathode potential of about 25 kV. This is achieved by filling the transformer with a compound. For the cathode heating transformer, the secondary winding is made of high-voltage conductive wire with combined insulation to increase the electrical strength. The electrical strength of the insulation between the primary and secondary windings is tested at 30 kV on an electrical breakdown system. The source parameters are measured. Waveforms showing the klystron cathode heater operation are presented in Figs. 5 and 6. Waveforms of the converter operating at the nominal input mains voltage are shown in Fig. 5; here, the yellow line (*1*) represents the voltage at the current sensor with a resistance of 0.51 Ohms (the vertical line is the voltage on a scale of 1 V/div), the green line (*2*) represents the voltage at the resonance capacitor (the vertical line is the voltage on a scale of 150 V/div), while the red line (*3*) represents the drain-to-source voltage of the upper transistor VT1. The horizontal line shows the time on a scale of 5 μs/div. It is clear from the waveforms shown that the voltage phase is ahead of the current phase and that the circuit is operating in the inductive region. Since the mains input voltage is stable, the converter operates close to the resonance frequency $f \approx 80$ kHz, which corresponds to the calculated values. In this mode, there is no need to change the operating frequency since the inverter parameters do not depend on the power consumption.

The transistor switching waveforms and the current sensor voltage at the input mains voltage of 198 V are shown in Fig. 6. The red (*1*) and yellow (*2*) lines represent the drain-to-source voltages of the upper VT1 and lower VT2 transistors, respectively (vertically, the voltage is on a scale of 200 V/div). The green line (*3*) shows the voltage at the current sensor (vertical is the voltage on a scale of 2 V/div). The horizontal line shows the time on a scale of 5 μs/div.

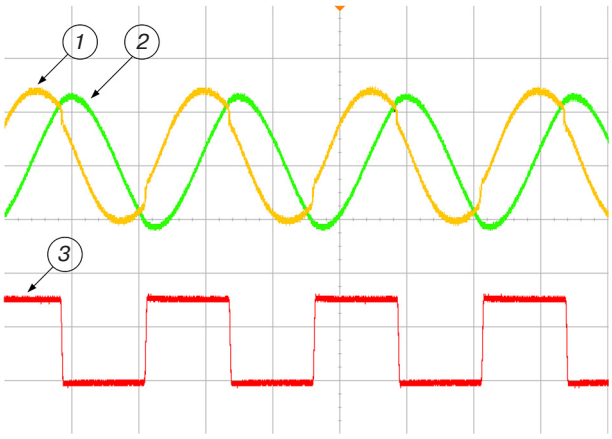

Fig. 5. Waveforms of the converter operating at rated input voltage

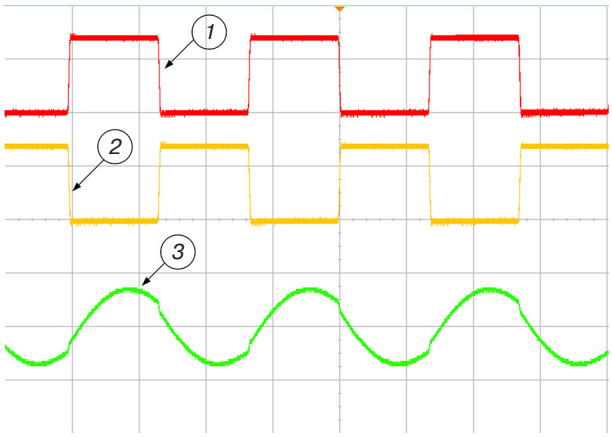

Fig. 6. Transistor switching waveforms at minimum input voltage

Similar to Fig. 6, Fig. 7 shows the inverter operating at maximum input voltage, which is 242 V.

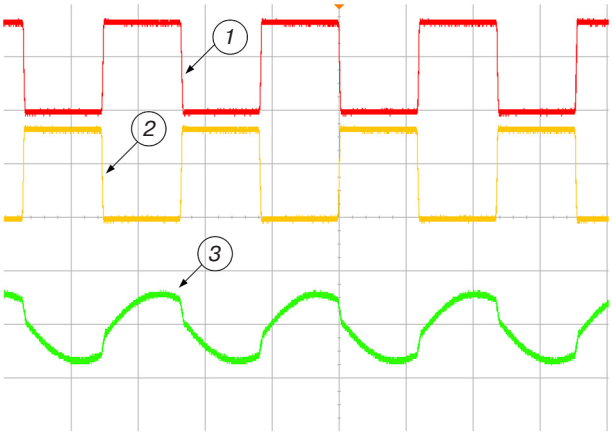

Fig. 7. Waveforms of the inverter operating at maximum input voltage

The zero-voltage switching mode is always implemented; the output voltage is maintained at the set level when the inverter is operated with different input voltages.

The operation of the converter can be divided into the following four stages:

1. Transistor VT1 is opened, the transformer primary current I_1 flows through the resonant circuit, and resonance occurs. When the resonance ceases, the current drops to the magnetizing current I_m.
2. Transistor VT1 is closed. The magnetizing current I_m continues to flow through the body diode of transistor VT2.
3. Transistor VT2 is opened, the energy stored in capacitor C_r generates current I_1 in the reverse direction, and the magnetizing current I_m crosses the zero point and increases in the reverse direction. Resonance occurs. When the resonance ceases, the current drops to the magnetizing current I_m.
4. Transistor VT2 is closed, and the magnetizing current I_m continues to flow through the body diode of transistor VT1. Transistor VT1 opens and the process is repeated.

In step 2, current flows through the body diode of transistor VT2, then the transistor opens when its drain-to-source voltage is close to zero (zero voltage switching). Similarly, transistor VT1 switches at zero voltage in step 4.

The measured efficiencies of the cathode heating and bias sources are 85% and 92%, respectively.

The prototype model of the resonant power supply is tested in the laboratory as part of the complex test simulation test bench for the radio transmitter of the multifunctional radar station. The functional scheme of the test bench is shown in Fig. 8.

In the initial state, a bias voltage of −6 kV is applied to the CE klystron via the R2 resistor assembly, and the klystron is locked. The voltage at the CE with respect to the collector −30 kV is the sum of the voltages of the cathode and bias supplies connected in series. After the control pulse in the modulator opens the start-up channel, the klystron opens and amplifies the input microwave signal. The voltage at the CE with respect to the collector is −24 kV. At the end of the control pulse, the start channel closes, the breakdown channel opens, a voltage of −30 kV is applied to the CE with respect to the collector, and the klystron closes. This process is shown in the waveform in Fig. 9.

The red (bottom) line shows the voltage at the CE relative to the klystron collector (vertically, the voltage is on a scale of 5 kV/div). The violet (top) line shows the envelope of the microwave output signal (vertical is the voltage on a scale of 5 V/div). The horizontal line shows the time on a scale of 2 μs/div.

From the depicted waveforms, it can be seen that, when the klystron is locked, the voltage at the CE is −29.75 kV and stable at the specified level. The microwave output power of the klystron, which is also stable, meets the specified nominal power. It can therefore be concluded that the developed sources are suitable for use in prototype radio transmitters.

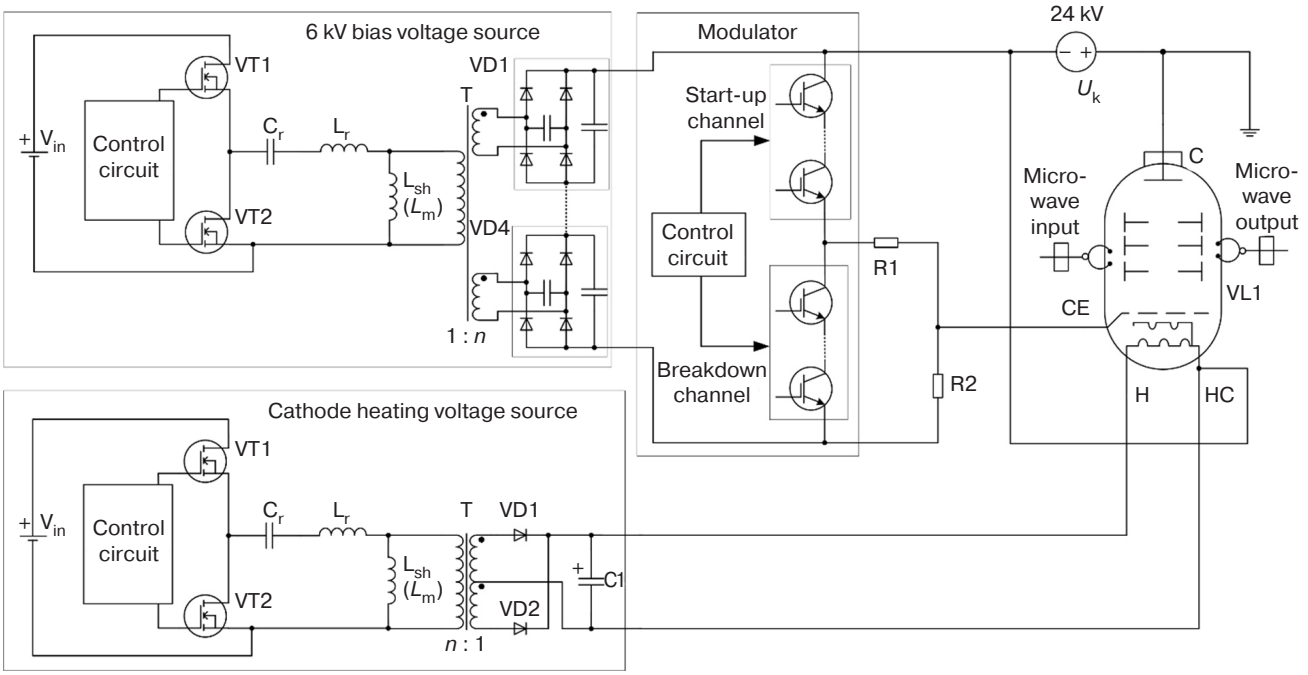

Fig. 8. Functional scheme of the test bench.
CE is the control electrode; H is the heater; HC is the heater-cathode; C is the collector; VL1 is the klystron; R1 is the current limiting resistor assembly; R2 is the bias pull-up resistor assembly; U_k is the power supply voltage of the klystron cathode

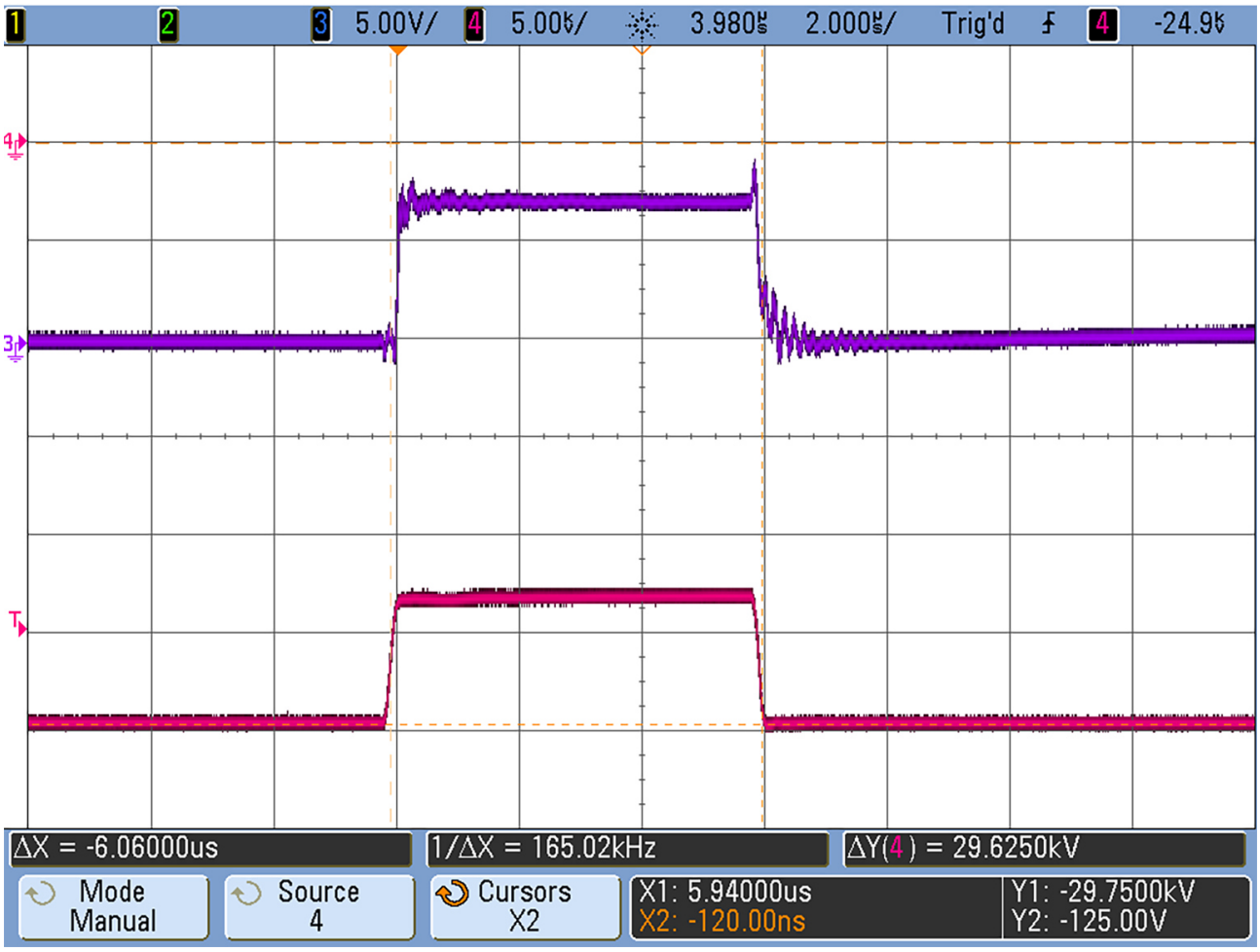

Fig. 9. Klystron operation

CONCLUSIONS

In the present work, a method for designing secondary power supplies for a vacuum microwave amplifier is proposed. The theory and calculation method of the resonant LLC source is presented. A method for calculating and carrying out transformer winding is discussed and tested. This method avoids the use of inductors as separate elements by integrating them into a magnetic system and providing decoupling by the high potential of the secondary winding.

The power supply is tested as part of a radio transmitter test bench complex. Waveforms of the cathode heater converter at minimum, nominal, and maximum input mains voltage are obtained. It is shown that the source operates in switching mode at zero voltage in the inductive region. The efficiencies of the cathode heating and bias sources are 85% and 92% respectively.

The developed power sources are smaller than transformer analogues and can maintain a stable output voltage when the input voltage changes, while the use of a soft start-up can help to extend the life of the klystron.

Authors' contribution

All authors have equally contributed to the research work.

REFERENCES

1. Sukhodolets L.G. *Moshchnye vakuumnye SVCh pribory* (*Powerful Vacuum Microwave Devices*). Textbook on the Study of Microwave Vacuum Devices. Moscow: IKAR; 2014. 272 p. (in Russ.).
2. Zabolotnaya S.V., Emelyanov E.V., Tsytsarev A.Yu., Albutov A.N. Automatic control, monitoring and protection system of multifunctional radar transmitter output amplifier. *Vestnik vozdushno-kosmicheskoi oborony = Aerospace Defense Herald*. 2017;2(14):70–76 (in Russ.). https://elibrary.ru/ysdqqr
3. Lobov I.N., Berezin O.K. A High-voltage pulse modulator for the MFR transmitter. *Vestnik vozdushno-kosmicheskoi oborony = Aerospace Defense Herald*. 2020;3(27):22–30 (in Russ.). https://www.elibrary.ru/atttkk
4. Baranov V.V., Lobov I.N., Khafizov D.R. High-voltage pulse modulator for a traveling wave lamp of radio transmitting equipment MRL. *Vestnik vozdushno-kosmicheskoi oborony = Aerospace Defense Herald*. 2023;2(38):55–62 (in Russ.). https://www.elibrary.ru/cqkgfd
5. Zinov'ev G.S. *Osnovy silovoi elektroniki* (*Fundamentals of Power Electronics*). Part 2. Novosibirsk: NGTU; 2000. 197 p. (in Russ.).
6. Polishchuk A. Highly efficient sources of secondary high-voltage power supply for microwave radio transmitters. *Silovaya Elektronika*. 2004;2:66–70 (in Russ.). https://elibrary.ru/mvrpnb
7. Lee S.-S., Moon G.-W. Full ZVS-Range Transient Current Buildup Half-Bridge Converter with Different ZVS Operations to Load Variation. *IEEE Trans. Ind. Electron*. 2008;55(6):2557–2559. https://doi.org/10.1109/TIE.2008.921239
8. Steigerwald R.L. A Comparison of Half-Bridge Resonant Converter Topologies. *IEEE Trans. Power Electron*. 1988;3(2): 174–182. http://doi.org/10.1109/63.4347
9. Zhang B., Zhao M., Huang P., Wang Q. Optimal design of GaN HEMT based high efficiency LLC converter. *Energy Rep*. 2022;8(5):1181–1190. https://doi.org/10.1016/j.egyr.2022.02.276
10. Zhang S., Li L., Zhao Z., Fan S., Wang C. Optimal trajectory based start-up control of LCC resonant converter for X-ray generator applications. *Energy Rep*. 2022;8(5):957–965. https://doi.org/10.1016/j.egyr.2022.02.266
11. Wei Y., Luo Q., Mantooth H.A. Synchronous Rectification for LLC Resonant Converter: An Overview. *IEEE Trans. Power Electron*. 2021;36(6):7264–7280. https://doi.org/10.1109/TPEL.2020.3040603
12. Li N., Cao Y., Zhang Y., Li Z., Jiang L., Zhang X.P. Parameter optimization strategy of LLC converter soft start-up process based on a simplified numerical calculation model. *Energy Rep*. 2023;9(10):909–919 https://doi.org/10.1016/j.egyr.2023.05.118
13. Kucka J., Dujic D. Equal Loss Distribution in Duty-Cycle Controlled H-Bridge LLC Resonant Converters. *IEEE Trans. Power Electron*. 2021;36(5):4937–4941. https://doi.org/10.1109/TPEL.2020.3028879
14. Smirnova V. A highly efficient, compact resonant ZVS bridge converter based on a 1200 V SiC MOSFET. *Silovaya Elektronika*. 2016;6(63):54–60 (in Russ.). https://elibrary.ru/xrngcd
15. Novikov Yu., Solomatin M. Development of a half-bridge resonant converter based on IRS2795. *Elektronnye komponenty*. 2011;3:103–111 (in Russ.).
16. Duerbaum T. First harmonic approximation including design constraints. In: *INTELEC – Twentieth International Telecommunications Energy Conference* (*Cat. No.98CH36263*). 1998. P. 321–328. https://doi.org/10.1109/INTLEC.1998.793519
17. Skuto A., Gaito A. The choice of a half-bridge resonant LLC converter and a MOSFET of the primary side. *Silovaya Elektronika*. 2016;2(59):30–32 (in Russ.). https://elibrary.ru/waoxqt
18. Semenov B.Yu. *Silovaya elektronika ot prostogo k slozhnomu* (*Power Electronics from Simple to Complex*). Moscow: SOLON-Press; 2005. 416 p. (in Russ.).
19. Chen Q., Long X., Chen Y., Xu S., Chen W. The Structure and Its Leakage Inductance Model of Integrated LLC Transformer With Wide Range Value Variation. *CPSS Trans. Power Electron. Appl*. 2022;7(4):409–420. https://doi.org/10.24295/CPSSTPEA.2022.00037
20. Khnykov A.V. *Teoriya i raschet transformatorov istochnikov vtorichnogo elektropitaniya* (*Theory and Calculation of Transformers of Secondary Power Supply Sources*). Moscow: SOLON-Press; 2004. 128 p. (in Russ.).

СПИСОК ЛИТЕРАТУРЫ

1. Суходолец Л.Г. *Мощные вакуумные СВЧ приборы.* Учебное пособие по изучению ЭВП СВЧ. М.: ИКАР; 2014. 272 с.
2. Заболотная С.В., Емельянов Е.В., Цыцарев А.Ю., Албутов А.Н. Система автоматизированного управления, защиты и контроля выходного усилителя передающего устройства многофункционального радиолокатора. *Вестник воздушно-космической обороны*. 2017;2(14):70–76. https://elibrary.ru/ysdqqr
3. Лобов И.Н., Березин О.К. Высоковольтный импульсный модулятор для аппаратуры передающего устройства МФР. *Вестник воздушно-космической обороны*. 2020;3(27):22–30. https://www.elibrary.ru/atttkk
4. Баранов В.В., Лобов И.Н., Хафизов Д.Р. Высоковольтный импульсный модулятор для лампы бегущей волны радиопередающей аппаратуры МРЛС. *Вестник воздушно-космической обороны*. 2023;2(38):55–62. https://www.elibrary.ru/cqkgfd
5. Зиновьев Г.С. *Основы силовой электроники. Часть 2*. Новосибирск: НГТУ; 2000. 197 с.

6. Полищук А. Высокоэффективные источники вторичного электропитания высокого напряжения для радиопередающих устройств СВЧ. *Силовая электроника*. 2004;2:66–70. https://elibrary.ru/mvrpnb
7. Lee S.-S., Moon G.-W. Full ZVS-Range Transient Current Buildup Half-Bridge Converter with Different ZVS Operations to Load Variation. *IEEE Trans. Ind. Electron*. 2008;55(6):2557–2559. https://doi.org/10.1109/TIE.2008.921239
8. Steigerwald R.L. A Comparison of Half-Bridge Resonant Converter Topologies. *IEEE Trans. Power Electron*. 1988;3(2): 174–182. http://doi.org/10.1109/63.4347
9. Zhang B., Zhao M., Huang P., Wang Q. Optimal design of GaN HEMT based high efficiency LLC converter. *Energy Rep*. 2022;8(5):1181–1190. https://doi.org/10.1016/j.egyr.2022.02.276
10. Zhang S., Li L., Zhao Z., Fan S., Wang C. Optimal trajectory based start-up control of LCC resonant converter for X-ray generator applications. *Energy Rep*. 2022;8(5):957–965. https://doi.org/10.1016/j.egyr.2022.02.266
11. Wei Y., Luo Q., Mantooth H.A. Synchronous Rectification for LLC Resonant Converter: An Overview. *IEEE Trans. Power Electron*. 2021;36(6):7264–7280. https://doi.org/10.1109/TPEL.2020.3040603
12. Li N., Cao Y., Zhang Y., Li Z., Jiang L., Zhang X.P. Parameter optimization strategy of LLC converter soft start-up process based on a simplified numerical calculation model. *Energy Rep*. 2023;9(10):909–919. https://doi.org/10.1016/j.egyr.2023.05.118
13. Kucka J., Dujic D. Equal Loss Distribution in Duty-Cycle Controlled H-Bridge LLC Resonant Converters. *IEEE Trans. Power Electron*. 2021;36(5):4937–4941. https://doi.org/10.1109/TPEL.2020.3028879
14. Смирнова В. Высокоэффективный, компактный резонансный ZVS мостовой конвертер на основе 1200 В SiC-MOSFET. *Силовая электроника*. 2016;6(63):54–60. https://www.elibrary.ru/xrngcd
15. Новиков Ю., Соломатин М. Разработка полумостового резонансного преобразователя на основе IRS2795. *Электронные компоненты*. 2011;3:103–111.
16. Duerbaum T. First harmonic approximation including design constraints. In: *INTELEC – Twentieth International Telecommunications Energy Conference* (*Cat. No. 98CH36263*). 1998. P. 321–328. https://doi.org/10.1109/INTLEC.1998.793519
17. Скуто А., Гайто А. Выбор полумостового резонансного LLC-преобразователя и MOSFET первичной стороны. *Силовая электроника*. 2016;2(59):30–32. https://elibrary.ru/waoxqt
18. Семенов Б.Ю. *Силовая электроника от простого к сложному*. М.: СОЛОН-Пресс; 2005. 416 с.
19. Chen Q., Long X., Chen Y., Xu S., Chen W. The Structure and Its Leakage Inductance Model of Integrated LLC Transformer With Wide Range Value Variation. *CPSS Trans. Power Electron. Appl*. 2022;7(4):409–420. https://doi.org/10.24295/CPSSTPEA.2022.00037
20. Хныков А.В. *Теория и расчет трансформаторов источников вторичного электропитания*. М.: СОЛОН-Пресс; 2004. 128 с.

About the authors

Damir R. Hafizov, Engineer, A.A. Raspletin NPO Almaz (80/16, Leningradskii pr., Moscow, 125190 Russia); Postgraduate Student, Department of Nanoelectronics, Institute for Advanced Technologies and Industrial Programming, MIREA – Russian Technological University (78, Vernadskogo pr., Moscow, 119454 Russia). E-mail: hafizov98@yandex.ru. RSCI SPIN-code 3037-0537, https://orcid.org/0009-0004-2662-0299

Ilya N. Lobov, Head of the Department, A.A. Raspletin NPO Almaz (80/16, Leningradskii pr., Moscow, 125190 Russia). E-mail: lobov.en@mail.ru. https://orcid.org/0009-0003-6741-825X

Leonid Y. Fetisov, Dr. Sci. (Phys.-Math.), Professor, Department of Nanoelectronics, Institute for Advanced Technologies and Industrial Programming, MIREA – Russian Technological University (78, Vernadskogo pr., Moscow, 119454 Russia). E-mail: fetisovl@yandex.ru. Scopus Author ID 26431336600, ResearcherID D-1163-2013, RSCI SPIN-code 9788-0680, https://orcid.org/0000-0002-3699-4321

Об авторах

Хафизов Дамир Ринатович, инженер, ПАО «НПО «Алмаз» имени академика А.А. Расплетина (125190, Россия, Москва, Ленинградский пр-т, д. 80, корп. 16); аспирант, кафедра наноэлектроники, Институт перспективных технологий и индустриального программирования, ФГБОУ ВО «МИРЭА – Российский технологический университет» (119454, Россия, Москва, пр-т Вернадского, д. 78). E-mail: hafizov98@yandex.ru. SPIN-код РИНЦ 3037-0537, https://orcid.org/0009-0004-2662-0299

Лобов Илья Николаевич, начальник отдела, ПАО «НПО «Алмаз» имени академика А.А. Расплетина (125190, Россия, Москва, Ленинградский пр-т, д. 80, корп. 16). E-mail: lobov.en@mail.ru. https://orcid.org/0009-0003-6741-825X

Фетисов Леонид Юрьевич, д.ф.-м.н., доцент, профессор кафедры наноэлектроники, Институт перспективных технологий и индустриального программирования, ФГБОУ ВО «МИРЭА – Российский технологический университет» (119454, Россия, Москва, пр-т Вернадского, д. 78). E-mail: fetisovl@yandex.ru. Scopus Author ID 26431336600, ResearcherID D-1163-2013, SPIN-код РИНЦ 9788-0680, https://orcid.org/0000-0002-3699-4321

Translated from Russian into English by K. Nazarov
Edited for English language and spelling by Thomas A. Beavitt